Tuning of magnetic frustration and emergence of a magnetostructural transition in $Mn_{1-x}Cd_xCr_2O_4$

Abhishek Das,[1] Dheeraj Ranaut [©],[2] Pratap Pal [©],[1,3] Riju Pal [©],[4] Shubhadip Moulick,[4] Moumita Das,[5] Dinesh Topwal,[6,7] Prabhat Mandal,[4,5] Atindra Nath Pal [©],[4] K. Mukherjee,[2] and Debraj Choudhury [©][1,*]

[1]*Department of Physics, Indian Institute of Technology Kharagpur, West Bengal 721302, India*
[2]*School of Physical Sciences, Indian Institute of Technology Mandi, Mandi 175075, Himachal Pradesh, India*
[3]*Department of Materials Science and Engineering, University of Wisconsin, Madison, Wisconsin 53706, USA*
[4]*S. N. Bose National Center for Basic Sciences, Block-JD, Sector-III, Salt Lake, Kolkata 700106, India*
[5]*Saha Institute of Nuclear Physics, HBNI, 1/AF Bidhannagar, Kolkata 700064, India*
[6]*Homi Bhabha National Institute, Training School Complex, Anushakti Nagar, Mumbai 400094, India*
[7]*Institute of Physics, Sachivalaya Marg, Bhubaneswar 751005, India*

$Mn_{1-x}Cd_xCr_2O_4$ spinel series is engineered to host a controlled and wide-range tuning of magnetic frustration through a nonmagnetic ion (Cd) doping in $MnCr_2O_4$ spinel oxide. While $MnCr_2O_4$ exhibits weak geometric magnetic frustration (GMF), the doping brings in an interplay between various competing magnetic-exchange interactions involving the Jahn-Teller inactive $Cr^{3+}(3d^3)$ spins that lie on a frustrated pyrochlore lattice in cubic spinel oxide. Magnetic frustration is observed to be the maximum for the intermediate values of x which are associated with large spin-relaxation times and an evolution in the nature of glassy spin dynamics. The dominant antiferromagnetic coupling between the Mn sites and Cr sites (which induces the intra-Cr-lattice spins to be nearly ferromagnetically coupled in $x = 0$) becomes weaker due to magnetic dilution of the Mn site by diamagnetic Cd^{2+} ions. As a result, the net interactions between Cr^{3+} ions in the pyrochlore lattice become antiferromagnetic beyond $x \gtrsim 0.6$. This causes the associated GMF to become very large for $x \gtrsim 0.6$. As a result, while the structure remains cubic till the lowest temperature for $0 \leqslant x \leqslant 0.60$, the appearance of strong GMF induces spin-driven magnetostructural transitions from a high-temperature cubic (paramagnetic) to a low-temperature tetragonal (and antiferromagnetic) phase. The obtained results demonstrate a direct link between GMF and spin-lattice coupling and provide a road map to design compounds with engineered magnetostructural transitions associated with large spin-lattice coupling.

I. INTRODUCTION

Investigations on compounds exhibiting strong spin-lattice coupling are paramount from a basic research perspective to elucidate the underlying driving mechanism and are also extremely promising for a plethora of applications, such as enhanced magnetocaloric effect [1–4], large magnetoelectric effect [5–7], anisotropic thermal transport [8], and many more. While such materials are relatively rare, compounds possessing large geometric magnetic frustration (GMF) often exhibit large spin-lattice coupling [9–11], although an explicit dependency remains to be demonstrated to the best of our knowledge. The phenomenon of GMF arises when various magnetic-exchange interactions of a material cannot simultaneously be optimized due to the geometry of the underlying crystalline lattice. This results in many possible ground states instead of a single magnetic ground state and the absence of any long-range magnetic ordering [12–15].

Transition-metal AB_2O_4 cubic spinel oxides present a classic example of such a geometrically frustrated lattice in which magnetic B-site ions alone lie on the edges of a three-dimensional network of corner-sharing tetrahedra, also referred to as a pyrochlore lattice, as shown in Fig. S1 of the Supplemental Material [16]. The B-site pyrochlore lattice is known to host one of the strongest GMFs in the presence of dominant antiferromagnetic interaction between the B-site spins [17–20]. In the presence of magnetic A- or B-site ions with orbital degrees of freedom in the corresponding high-symmetry cubic phases (as in $FeCr_2O_4$ possessing Jahn-Teller (JT) active $Fe^{2+}(3d^6)$ ion [21–23]; $MnTi_2O_4$ with JT-active $Ti^{3+}(3d^1)$ ion [24,25]), JT distortion driven symmetry-lowering structural transition helps in distorting the frustrated pyrochlore lattice and this enables one to stabilize a long-range magnetic ordering. Interesting physics emerge in AB_2O_4 spinels possessing JT-inactive A- and B-site ions (such as $ZnCr_2O_4$, which contains diamagnetic $Zn^{2+}(3d^0)$ and magnetic $Cr^{3+}(3d^3)$ ions [26,27]), where, in the absence of orbital degeneracy, pure spin-driven structural changes (referred to as the spin-JT effect) can become effective to reduce the GMF and enable long-range magnetic ordering. The extent of such spin-induced structural modifications (i.e., the spin-JT effect) or the spin-lattice coupling vary strongly among the ACr_2O_4 spinels containing JT-inactive ions; it is found to be strong in those involving nonmagnetic A-site ions [like $Zn^{2+}(3d^0)$ and $Cd^{2+}(4d^0)$ ions] [26–29] and weak

*debraj@phy.iitkgp.ac.in
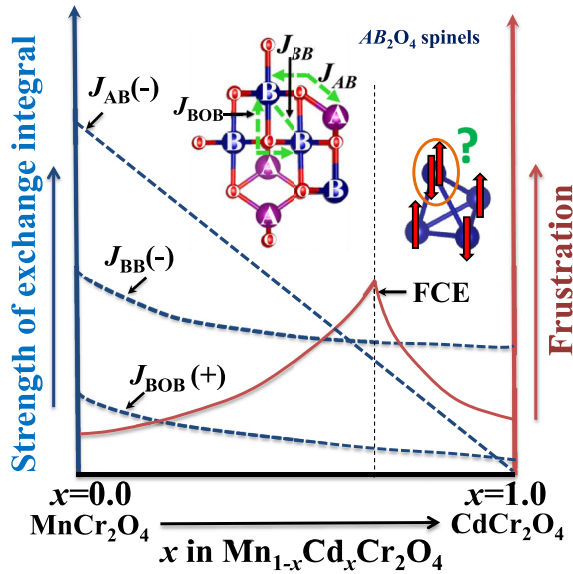
FIG. 1. Qualitative representation of the expected evolution of different exchange integrals and frustration indexes in the $Mn_{1-x}Cd_xCr_2O_4$ series. The right-hand inset shows a corner-shared tetrahedra unit with Cr atoms. This kind of geometry causes huge GMF, when spins try to interact antiferromagnetically. The left-hand inset highlights the different interactions that arise in AB_2O_4 spinels. While $J_{BB}(-)$ and $J_{B0B}(+)$ denote antiferromagnetic direct-exchange and ferromagnetic superexchange interactions between Cr^{3+} ions, J_{AB} denotes the antiferromagnetic superexchange interaction between Cr^{3+} and Mn^{2+} ions.

in those involving magnetic A-site ions [like $Mn^{2+}(3d^5)$ and $Co^{2+}(3d^7)$ ions] [30]. In order to investigate whether it is possible to controllably increase the strength of the spin-JT effect and demonstrate its explicit dependency on GMF, we investigate the $Mn_{1-x}Cd_xCr_2O_4$ series. The weak spin-JT effect in the $x = 0$ member, i.e., $MnCr_2O_4$ [30], which involves weak structural changes around the high-temperature spin-glass transition, is likely driven by its corresponding weak GMF [31]. In $MnCr_2O_4$, the net alignment of the pyrochlore-lattice Cr spins is mainly governed by the much larger A-site Mn^{2+} (5 μ_B) spin moments. Among the multiple exchange pathways involving the Cr ions (illustrated in Fig. 1), the antiferromagnetic Mn-O-Cr intersite superexchange interaction (J_{AB}) dominates over the net antiferromagnetic Cr-Cr interaction [32]. The net Cr-Cr magnetic interaction comes out to be antiferromagnetic since the Cr-Cr antiferromagnetic direct-exchange (J_{BB}) supersedes the ferromagnetic Cr-O-Cr superexchange interaction (J_{BOB}) owing to the smaller Cr-Cr distance in $MnCr_2O_4$. However, due to the dominant Mn-O-Cr superexchange interaction, the net spin alignment between the Cr spins is nearly ferromagnetic (albeit along with small transverse Cr spin components [30,31,33]), which helps in significantly reducing the GMF in $MnCr_2O_4$. Progressive doping by a larger and nonmagnetic Cd^{2+} ion in place of the smaller and magnetic Mn^{2+} ion in $Mn_{1-x}Cd_xCr_2O_4$ is attempted with the expectations (illustrated in Fig. 1) that with increasing x (i) the Cr-Cr bond distance and the Cr-O-Cr bond angle will gradually increase, causing a weakening of J_{BB} direct-exchange and J_{BOB} superexchange interactions; (ii)

the magnitude of J_{AB} will likely linearly reduce due to the magnetic dilution of the A-site; (iii) around the x value where J_{AB} (that drives ferromagnetic alignment between Cr ions) just becomes smaller than $J_{BB} + J_{BOB}$ (which tends to drive antiferromagnetic alignment between Cr spins), the frustration due to competing interactions (FCE) will peak due to comparable opposing magnetic interactions; and (iv) since the net Cr-Cr interaction becomes antiferromagnetic beyond this x, the higher x compounds will be associated with a large GMF and possibly a large spin-JT effect. The obtained results are indeed in accordance with the above expectations and do exhibit the emergence of spin-driven global structural transitions for higher x members in the $Mn_{1-x}Cd_xCr_2O_4$ series.

II. METHODOLOGY

Polycrystalline $Mn_{1-x}Cd_xCr_2O_4$ ($0 \leqslant x \leqslant 1$) samples were synthesized using a solid state reaction: the well-grounded stoichiometric mixtures of Cr_2O_3, MnO, and CdO were sintered inside evacuated quartz tubes at 1150 °C for 24 h. Temperature-dependent phase formations, chemical homogeneity, and compositions were investigated using x-ray diffraction (XRD) with a Cu-$K\alpha$ source and energy-dispersive analyses of x rays (EDAX), respectively. All samples were found to be nearly phase pure (as shown in the wide-angle XRD spectra in Fig. S2 of Ref. [16]) with trace quantities of the Cr_2O_3 impurity phase. The room-temperature cubic (Fd-3m) lattice parameters and the Cr_2O_3 impurity percentages (~1%), determined from Rietveld refinement analyses (a representative refinement of the XRD spectrum for $x = 0.4$ is shown in Fig. S3 of Ref. [16]) of the XRD spectra using FullProf software [34], are included in Table I of Ref. [16]. The synthesized samples were found to be chemically homogeneous and the obtained atomic percentages (as determined from EDAX experiments) were very close to the corresponding nominal percentages, as shown in Table II of Ref. [16]. Temperature-dependent dc and ac magnetic properties were investigated using a superconducting quantum interference device (SQUID) magnetometer from Quantum Design. Dielectric measurements were carried out with the help of an LCR meter and an impedance analyzer.

III. RESULTS AND DISCUSSIONS

In consistency with the larger size of the doped Cd^{2+} ion (ionic radius ~0.78 Å) in place of the smaller Mn^{2+} ion (ionic radius ~0.66 Å) in $Mn_{1-x}Cd_xCr_2O_4$, a systematic shift in the (311) main XRD peak's position to lower angles is observed with increasing x [as shown in Fig. 2(a)]. This results in a monotonic increase of the cubic lattice parameter with increasing x [shown in Fig. 2(b)], in accordance with Vegard's law. Also, this leads to the predicted systematic increase in the corresponding Cr-Cr bond distance and Cr-O-Cr (away from 90°) bond angle (which causes a resultant decrease in the Cr-O-Mn bond angle below 120°) with increasing x, as obtained from structural refinements and shown in Figs. 2(c) and 2(d).

To investigate the role of these structural modifications and progressive magnetic dilution on the magnetic properties of $Mn_{1-x}Cd_xCr_2O_4$, temperature- and magnetic-field-dependent
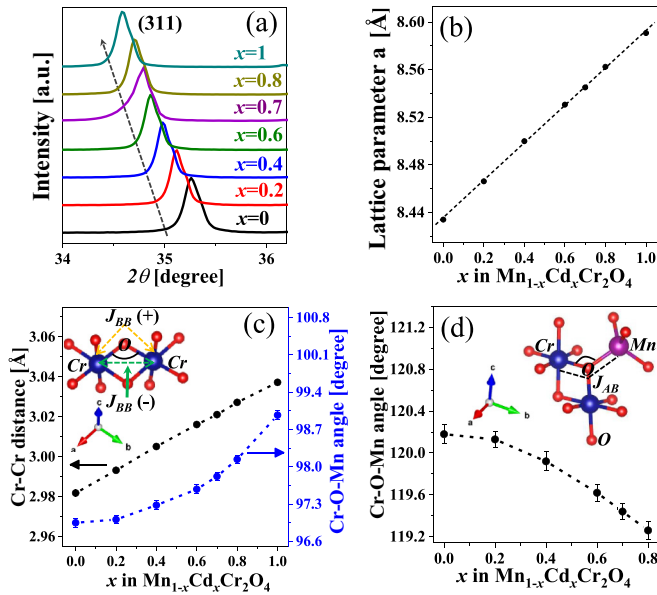
FIG. 2. (a) Evolution of the (311) cubic Bragg peak with x. Variation of (b) the lattice parameter, (c) the Cr-Cr distance and the Cr-O-Cr angle, and (d) the Cr-O-Mn angle with x at room temperature. The inset of panel (c) shows a pair of edge-shared CrO_6 octahedra in the cubic phase (Fd-$3m$) of $Mn_{1-x}Cd_xCr_2O_4$ ($0 \leqslant x \leqslant 1$). A schematic of the corner-shared CrO_6 octahedra and the MnO_4 tetrahedra connected by oxygen is highlighted in the inset of panel (d).

dc magnetization (M) and ac magnetic susceptibility measurements were carried out. As seen in the dc magnetization as a function of temperature plot in Fig. 3(a) (the magnetization plot for $x = 0.7$ is shown in Fig. S4 of Ref. [16]), the $x = 0$ member (i.e., $MnCr_2O_4$) undergoes three successive magnetic transitions (in accordance with earlier magnetization results [30,31,35]), which are a ferrimagnetic transition at $T_{N1} \sim 43$ K followed by lower-temperature glassy magnetic transitions at $T_{N2} \sim 18$ K (short-range spiral ordering) and $T_{N3} \sim 10$ K (lock-in transition). The corresponding ac magnetic susceptibility data help in elucidating an additional higher-temperature magnetic ordering at T_{SP} (higher than T_{N1}) for $x = 0$, as shown in Fig. 3(c), which is not visible in the corresponding dc magnetization data due to the large background signal [30]. Nevertheless, $0 \leqslant x \leqslant 0.6$, and the evolution of all the three magnetic transitions, i.e., at T_{SP}, T_{N1}, and T_{N2}, can be traced through corresponding peak positions in the temperature derivative of the dc magnetization data (shown in Fig. S5 of Ref. [16]) and peaks in the corresponding ac susceptibilty plots in Fig. 3(c) (the lowest-temperature transition at T_{N3} cannot be detected for higher-x members). The expected monotonic decrease in the ordering temperatures T_{SP}, T_{N1}, and T_{N2} with increasing x (due to the magnetic dilution effect and from the changes as illustrated in Fig. 1) are clearly discernible, as indicated by the arrow marks in Figs. 3(a) and 3(c).

Similar to $x = 0$, the ferrimagnetic transition at T_{N1} for $0 < x \leqslant 0.6$ continues to be of a long-range nature. The long-range nature of the transition is confirmed through the dispersionless nature of the corresponding peak positions of

the real (χ') and imaginary (χ'') parts of the ac magnetic susceptibility between various magnetic-field frequencies [as shown in Figs. 4(a)–4(e) and Fig. S6 of Ref. [16] for the compounds with $0 \leqslant x \leqslant 0.6$]. Also, in accordance with $x = 0$ [30], the higher-temperature transition at T_{SP} and the lower-temperature transition at T_{N2} for $0 < x \leqslant 0.6$ are found to be glassy in nature. The glassy nature becomes evident from the susceptibility plots, as the corresponding χ' and χ'' peaks disperse strongly on varying the magnetic-field frequencies [the frequency dispersive nature of the magnetic transitions at T_{SP} is highlighted in the insets of Figs. 4(a)–4(d) and the same at T_{N2} is highlighted in Fig. 4(e) (for $x = 0.2$) and Fig. S6 of Ref. [16]; the T_{N2} peak likely falls close to our lowest measurement temperature for $x = 0.6$]. The glassy nature of the magnetic transitions at T_{SP} and T_{N2} are also confirmed by the presence of associated memory and aging effects as determined by employing dc memory effects (detailed methodology and results included in Sec. IX and Fig. S7 of Ref. [16], respectively). Importantly, the observation of a higher-temperature glassy magnetic transition at T_{SP} followed by a long-range ferrimagnetic ordering at T_{N1} also suggests the presence of weak spin-JT-effect-driven structural modifications at intermediate temperatures for $0 < x \leqslant 0.6$ as observed in $x = 0$ [30]. Such structural modifications have been demonstrated to become crucial to reducing the GMF and enabling long-range magnetic ordering at T_{N1} [30]. To probe the nature of the glassy magnetic transitions at T_{SP} and T_{N2}, a critical slowing-down analysis of the dependence of the relaxation time (τ) on the freezing temperature (T_F) (using the power-law model $\tau = \tau_o(\frac{T_f}{T_g} - 1)^{-z\nu}$ [36], the detailed discussion is given in Sec. XI of Ref. [16]) was employed. To further verify, the empirical Mydosh parameter (K) [37] analysis [$K = \frac{\Delta T_F(\omega)}{T_F \Delta \ln \omega}$, where ΔT_F is the difference between the χ' peak temperatures (T_F) corresponding to the lowest and highest magnetic-field angular frequencies (ω)] was performed. The extracted parameter values from the best fits to the critical slowing-down model [shown for $x = 0.2$ (associated with the magnetic transition at T_{N2}) in Fig. 4(f) and in Figs. S8 and S9 of Ref. [16] for other x members] and the obtained Mydosh parameters are listed in Table III of Ref. [16]. The values of these parameters clearly suggest T_{N2} to be a cluster-glass [37–41] transition for $0 \leqslant x \leqslant 0.6$. In regards to the higher-temperature glass transition at T_{SP}, the obtained τ_o value continues to increase between $x = 0$ to $x = 0.6$ (as shown in Table III of Ref. [16]). Notably, the extracted τ_o values clearly suggest T_{SP} to be a spin-glass transition [37,42–46] for $x = 0$ and 0.2 and a cluster-glass transition for $x = 0.4$ and 0.6. Interestingly, the evolution of T_{SP} from a spin-glass to a cluster-glass transition [which later is associated with large relaxation times (τ_o)] with increasing x suggests the presence of a larger magnetic frustration in the later compositions that causes the associated spin dynamics to become more sluggish and lead to larger spin-relaxation times.

Qualitatively different magnetic properties are observed for $x > 0.6$, which exhibit a single long-range antiferromagnetic (which is confirmed through corresponding dispersionless χ' peaks for $x = 0.8$ and 1, as shown in Figs. 5(a) and 5(b), respectively) transition at T_N instead of multiple magnetic transitions as seen for the lower-x members [see Figs. 3(a)
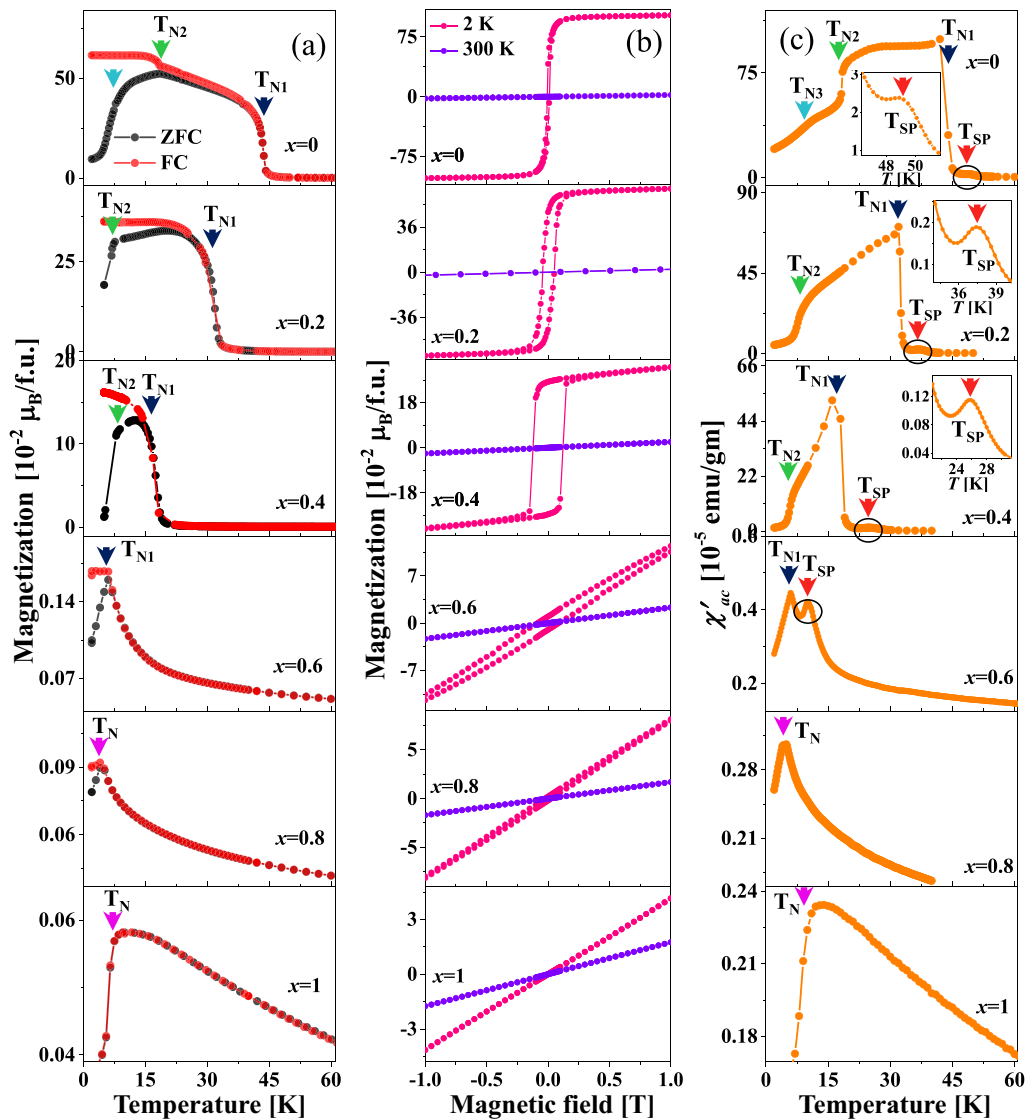
FIG. 3. (a) Temperature dependence of dc magnetization (M) of $Mn_{1-x}Cd_xCr_2O_4$ ($0 \leqslant x \leqslant 1$), studied both after zero-field cooling (ZFC) and field cooling (FC) with an applied magnetic field (H) of 100 Oe. (b) Isothermal M-H curves at 2 and 300 K. (c) Temperature dependence of the real (in-phase) part of ac susceptibility ($\chi\prime$), measured at a static magnetic field of 4 Oe and a driving ac field of 1 Oe. The magnified views of the weak magnetic transition near T_{SP} for $x = 0$, 0.2, and 0.4 are highlighted in the insets. The red, navy, green, sky blue, and purple arrows refer to the high-temperature glassy magnetic transition at T_{SP}, the ferrimagnetic transition at T_{N1}, the short-range spiral transition at T_{N2}, the lock-in transition at T_{N3}, and the antiferromagnetic transition at T_N, respectively.

and 3(c)]. The qualitative change in magnetic properties across $x = 0.6$ also becomes apparent from the shapes of the corresponding low-temperature M vs magnetic field (H) curves, as seen in Figs. 3(b) and the corresponding high-field M_{5T} values, as discussed in the following. A crossover from ferrimagnetic for $0 \leqslant x \leqslant 0.6$ to antiferromagneticlike coupling between the Cr spins for $x > 0.6$ becomes clearly discernible. While $x = 0$ exhibits soft ferrimagnetic (FIM) loop (i.e., nearly saturated high-field magnetization, negative intercept of inverse magnetic susceptibility data, as shown in Fig. S10(a) of Ref. [16] and finite, though, small magnetic coercivity), the magnetic coercivity gets more pronounced with increasing x up to $x = 0.4$. Beyond $x = 0.4$, the M-H loop starts to shrink and becomes almost linear for $x = 0.8$

and 1, characteristic of an antiferromagnet. The enhancement of coercive field in the ferrimagnetic phase for intermediate compositions around $x = 0.5$ is likely caused by an enhanced cationic disorder from doping and the pinning effects due to the presence of comparable FM and AFM interactions [47]. The experimentally determined high-field magnetization value (M_{5T}) corresponding to $H = 5$ T for $0 \leqslant x \leqslant 0.6$ can be reasonably understood by employing a ferrimagnetic model (as in $x = 0$) that considers (i) a near-ferromagnetic alignment (albeit with certain canting involved) of the Cr (B-site) spins and antiferromagnetically coupled to the Mn (A-site) spins and (ii) a monotonic reduction of the A-site magnetic moment due to progressive nonmagnetic Cd^{2+}-ion doping, as illustrated in Fig. 5(c). M_{5T} values for $x > 0.6$ deviate from
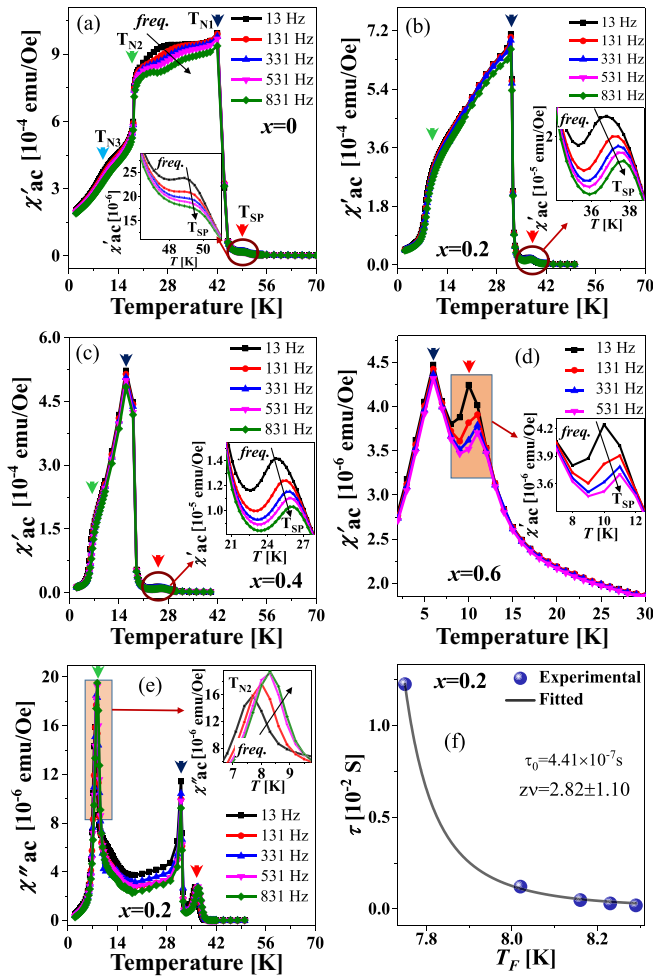
FIG. 4. Temperature dependence of the real (in-phase) part of ac susceptibility ($\chi\prime$) with multiple frequencies for (a) $x = 0$, (b) $x = 0.2$, (c) $x = 0.4$, and (d) $x = 0.6$. The corresponding frequency dispersive nature of the magnetic transition at T_{SP} is highlighted in the insets. (e) Temperature dependence of the imaginary (out-of-phase) part of ac susceptibility ($\chi\prime\prime$) with multiple frequencies for $x = 0.2$. The inset depicts the magnified view of the frequency dispersive nature of the magnetic transition near T_{N2}. (f) Variation of relaxation time (τ) with freezing temperature T_F associated with the frequency dispersive region near T_{N2} for $x = 0.2$. Blue spheres represent the experimental data, whereas the black solid line indicates the fitted curve.

FIG. 5. Temperature dependence of the real (in-phase) part of ac susceptibility ($\chi\prime$) with multiple frequencies for (a) $x = 0.8$ and (b) $x = 1$. (c) Variation of magnetization at 5 T (M_{5T}) with x. Deviation from linear ferrimagnetic dependency is indicated by the fitted green line. The left- and right-hand insets highlight the low-temperature spin configurations of MnCr$_2$O$_4$ and CdCr$_2$O$_4$, respectively. Panel (d) illustrates the fitting of the $1/\chi$ vs T plot for $x = 0.8$ using the Curie-Weiss law. The inset highlights the variation of frustration index (f) with x.

this linear x dependency in the ferrimagnetic state and are closer to that obtained for $x = 1$ (CdCr$_2$O$_4$), in which Cr spins are arranged in an incommensurate antiferromagnetic spiral configuration [48].

In order to have an qualitative estimation of the magnetic frustration arising from competing magnetic interactions (FCE) with increasing x, we have investigated the evolution of the frustration index ($f = \frac{\Theta}{T_N}$; a system is considered to be moderately frustrated when $1 < f < 10$ and strongly frustrated when $f > 10$.) [9,49–53] with x, determined from a Curie-Weiss analysis of inverse susceptibility data, as represented for $x = 0.8$ in Fig. 5(d) and for other x members in Sec. XII of Ref. [16]. Indeed, the estimated f values ex-

hibit a nonmonotonic dependency on x [as listed in Table IV of Ref. [16] and plotted in the inset to Fig. 5(d)] with a maximum value between $x = 0.6$ and 0.7. The observed nonmonotonic trend of f surprisingly agrees well with the anticipated dependency of FCE on x only (as shown in Fig. 1). Also, the observed dependence of f on x does not reflect the expected emergence of a large GMF for $x > 0.6$. This observation is significant as it suggests an alternate mechanism (like spin-induced structural phase transitions) that becomes effective in releasing the large GMF in the absence of any higher-temperature magnetic transition to enable long-range antiferromagnetic transition in the $x \gtrsim 0.6$ members.

The presence of strong spin-lattice coupling is also evident from the dielectric constant (ε_r) peak at T_N for $x = 1$ [54–57], while such a feature is absent across T_{N1} for the $x = 0$ sample, as seen in Fig. 6(a) and its inset. Interestingly, the ε_r peak at T_N for $x = 1$ does not disperse with varying field frequencies [as seen in Fig. 6(a)], which is suggestive of an accompanying structural transition. Anomalies at the magnetic transition temperatures are also visible in the specific heat data for $x = 0.2$ and $x = 0.8$ [as shown in Fig. 6(b)], where the transition at T_N for $x = 0.8$ appears sharper than that at T_{N1} for $x = 0.2$. To investigate any GMF-triggered emergent structural phase transition arising from large spin-lattice coupling for $x \gtrsim 0.6$, temperature-dependent XRD experiments were carried out on some representative x members from the two qualitatively different batches, namely, ferrimagnetic $x = 0.2$
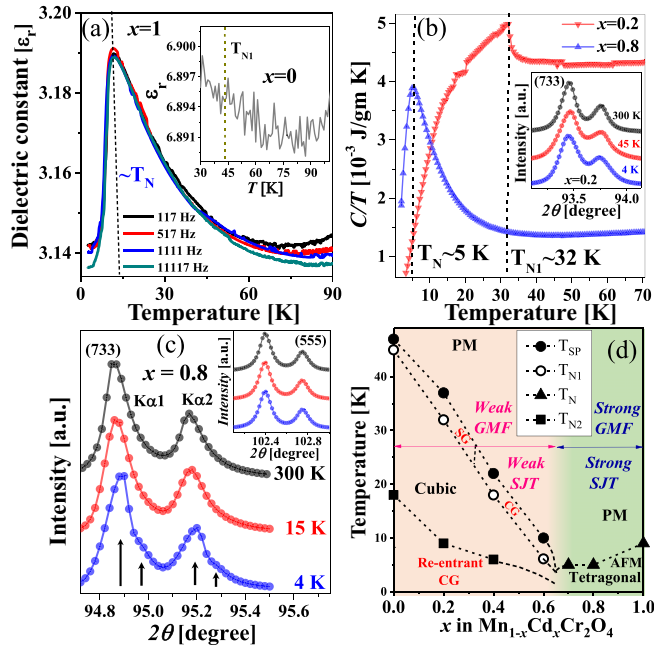
FIG. 6. (a) Dielectric constant vs temperature plots of $x = 1$. The same for $x = 0$ is shown in the inset. (b) Temperature variation of specific heat of $x = 0.2$ and 0.8. The inset depicts the absence of symmetry lowering for $x = 0.2$, as the (733) reflection does not split at 4 K. (c) Lowering of the crystal symmetry for $x = 0.8$ is evident by the splitting of the (733) cubic reflection into tetragonal (523) and (307) reflections at $T = 4$ K. The two distinct large peaks that correspond to the (733) reflection at 2θ values of $\sim 94.9°$ and $\sim 95.2°$ arise due to Cu-Kα1 and Cu-Kα2, respectively. The evolution of the (555) reflection at 300 and 4 K for $x = 0.8$ is shown in the inset of panel (c). (d) Obtained magnetostructural phase diagram of the $Mn_{1-x}Cd_xCr_2O_4$ series.

and antiferromagnetic $x = 0.7$ and 0.8. XRD measurements were performed at two temperatures, one below (at $T = 4$ K) and another above (at $T = 300$ K) the magnetic transition temperatures. While no temperature-dependent peak-shape change is detected for any of the XRD peaks for $x = 0.2$ [as seen in the inset of Fig. 6(b)], a clear peak splitting of the (733) XRD peak for $x = 0.8$ [as shown in Fig. 6(c)] and a peak broadening of the (842) peak for $x = 0.7$ (as shown in Fig. S11 of Ref. [16]) are observed only below T_N, which is indicative of a symmetry-lowering structural phase transition in the latter [58,59]. Notably, such a peak splitting,

however, cannot be observed for the (555) XRD peak below T_N for $x = 0.8$ [as shown in the inset of Fig. 6(c)]. Since the (555) XRD peak does not exhibit any splitting within a cubic or a tetragonal phase, but splits in an orthorhombic phase, the above observation clearly elucidates the emergence of a low-temperature tetragonal space group for $x \gtrsim 0.6$ below the corresponding T_N. The obtained results are summarized into a rich magnetostructural phase diagram, as shown in Fig. 6(d). For $0 \leqslant x \leqslant 0.6$, although multiple magnetic transitions are observed, the structure remains globally cubic down to the lowest temperature. In this x window, structural modifications (within an overall cubic structure) accompany the higher-temperature glassy magnetic transition at T_{SP} (as shown for $x = 0$) to reduce the already weakened GMF (as explained earlier). Instead, magneto-structural transitions are realized for $x \gtrsim 0.6$, where a spin-driven structural transition from a cubic to a tetragonal phase has been engineered to accompany the long-range antiferromagnetic transition. Unlike the continuous tuning of the magnetic frustration index (which varies gradually and goes through a maximum for intermediate-x compositions), GMF is not gradually tunable in $Mn_{1-x}Cd_xCr_2O_4$. The associated GMF takes either a small value, i.e., weak GMF in the x range $0 < x \leqslant 0.6$, or a large value, i.e., strong GMF for $x > 0.6$, as illustrated in the phase diagram [Fig. 6(d)] of $Mn_{1-x}Cd_xCr_2O_4$.

IV. CONCLUSIONS

In summary, through doping of nonmagnetic and larger Cd^{2+} ions in place of magnetic and smaller Mn^{2+} ions in $Mn_{1-x}Cd_xCr_2O_4$ ($0 \leqslant x \leqslant 1$), tunings of various exchange interactions involving the Cr ions that lie on a geometrically frustrated pyrochlore lattice have been successfully achieved. This facile tuning leads to nonmonotonic variation of the magnetic frustration with x and an emergence of a large GMF, which is associated with the onset of magnetostructural transitions, for higher-x members. The obtained results, thus, demonstrate a direct link between enhanced GMF and a strong spin-Jahn-Teller effect (or enhanced spin-lattice coupling) in this series.

[1] W. Choe, V. K. Pecharsky, A. O. Pecharsky, K. A. Gschneidner, Jr., V. G. Young, Jr., and G. J. Miller, Making and Breaking Covalent Bonds across the Magnetic Transition in the Giant Magnetocaloric Material Gd$_5$(Si$_2$Ge$_2$), Phys. Rev. Lett. **84**, 4617 (2000).

[2] V. K. Pecharsky, A. P. Holm, K. A. Gschneidner, and R. Rink, Massive Magnetic-Field-Induced Structural Transformation in Gd$_5$Ge$_4$ and the Nature of the Giant Magnetocaloric Effect, Phys. Rev. Lett. **91**, 197204 (2003).

[3] J. Liu, T. Gottschall, K. P. Skokov, J. D. Moore, and O. Gutfleisch, Giant magnetocaloric effect driven by structural transitions, Nat. Mater. **11**, 620 (2012).

[4] Y. Taguchi, H. Sakai, and D. Choudhury, Magnetocaloric materials with multiple instabilities, Adv. Mater. **29**, 1606144 (2017).

[5] K. Zhai, Y. Wu, S. Shen, W. Tian, H. Cao, Y. Chai, B. C. Chakoumakos, D. Shang, L. Yan, F. Wang, and Y. Sun, Giant magnetoelectric effects achieved by tuning spin cone symmetry in Y-type hexaferrites, Nat. Commun. **8**, 519 (2017).

[6] Z. Wang, N. Qureshi, S. Yasin, A. Mukhin, E. Ressouche, S. Zherlitsyn, Y. Skourski, J. Geshev, V. Ivanov, M. Gospodinov, and V. Skumryev, Magnetoelectric effect and phase transitions in CuO in external magnetic fields, Nat. Commun. **7**, 10295 (2016).

[7] M. Gen, A. Miyakei, H. Yagiuchi, Y. Watanabe, A. Ikeda, Y. H. Matsuda, M. Tokunaga, T. Arima, and Y. Tokunaga, Enhancement of giant magnetoelectric effect in Ni-doped $CaBaCo_4O_7$, Phys. Rev. B **105**, 214412 (2022).

[8] G. Qin, H. Wang, L. Zhang, Z. Qin, and M. Hu, Giant effect of spinlattice coupling on the thermal transport in two-dimensional ferromagnetic CrI_3, J. Mater. Chem. C **8**, 3520 (2020).

[9] A. P. Ramirez, Strongly geometrically grustrated magnets, Annu. Rev. Mater. Sci. **24**, 453 (1994).

[10] S.-H. Lee, C. Broholm, W. Ratcliff, G. Gasparovic, Q. Huang, T. H. Kim, and S.-W. Cheong, Emergent excitations in a geometrically frustrated magnet, Nature (London) **418**, 856 (2002).

[11] O. Tchernyshyov, R. Moessner, and S. L. Sondhi, Order by Distortion and String Modes in Pyrochlore Antiferromagnets, Phys. Rev. Lett. **88**, 067203 (2002).

[12] L. Balents, Spin liquids in frustrated magnets, Nature (London) **464**, 199 (2010).

[13] S. Kundu, A. Hossain, P. Keerthi S., R. Das, M. Baenitz, P. J. Baker, J.-C. Orain, D. C. Joshi, R. Mathieu, P. Mahadevan, S. Pujari, S. Bhattacharjee, A. V. Mahajan, and D. D. Sarma, Signatures of a Spin-1/2 Cooperative Paramagnet in the Diluted Triangular Lattice of Y_2CuTiO_6, Phys. Rev. Lett. **125**, 117206 (2020).

[14] Y. Okamoto, M. Nohara, H. Aruga-Katori, and H. Takagi, Spin-Liquid State in the $S = 1/2$ Hyperkagome Antiferromagnet $Na_4Ir_3O_8$, Phys. Rev. Lett. **99**, 137207 (2007).

[15] S. T. Bramwell and M. J. P. Gingras, Spin ice state in frustrated magnetic pyrochlore materials, Science **294**, 1495 (2001).

[16] See Supplemental Material at http://link.aps.org/supplemental/10.1103/PhysRevB.108.064426 for supporting structural and magnetization data. Rietveld refinements of the x-ray diffraction data, refined structural parameters and data related to EDX analyses are provided. Analyses of ac-susceptibility relaxations with critical slowing down model, fitting of dc-magnetization data with Curie-Weiss law, and ZFC memory data are also included.

[17] M. J. Harris and M. P. Zinkin, Frustration in the pyrochlore antiferromagnet, Mod. Phys. Lett. B **10**, 417 (1996).

[18] J. N. Reimers, Absence of long-range order in a three-dimensional geometrically frustrated antiferromagnet, Phys. Rev. B **45**, 7287 (1992).

[19] B. Canals and C. Lacroix, Pyrochlore Antiferromagnet: A Three-Dimensional Quantum Spin Liquid, Phys. Rev. Lett. **80**, 2933 (1998).

[20] R. Moessner and J. T. Chalker, Low-temperature properties of classical geometrically frustrated antiferromagnets, Phys. Rev. B **58**, 12049 (1998).

[21] S. Bordacs, D. Varjas, I. Kezsmark, G. Mihaly, L. Baldassarre, A. Abouelsayed, C.-A. Kuntscher, K. Ohgushi, and Y.

[22] Tokura, Magnetic-Order-Induced Crystal Symmetry Lowering in ACr_2O_4 Ferrimagnetic Spinels, Phys. Rev. Lett. **103**, 077205 (2009).

[22] V. Kocsis, D. Varjas, K. Penc, A. Abouelsayed, C. A. Kuntscher, K. Ohgushi, Y. Tokura, and I. Kezsmark, Magnetoelasticity in ACr_2O_4 spinel oxides (A = Mn, Fe, Co, Ni, and Cu), Phys. Rev. B **87**, 064416 (2013).

[23] J. Ma, V. O. Garlea, A. Rondinone, A. A. Aczel, S. Calder, C. Cruz, R. Sinclair, W. Tian, S. Chi, A. Kiswandhi, J. S. Brooks, H. D. Zhou, and M. Matsuda, Magnetic and structural phase transitions in the spinel compound $Fe_{1+x}Cr_{2-x}O_4$, Phys. Rev. B **89**, 134106 (2014).

[24] T. Sonehara, K. Kato, K. Osaka, M. Takata, and T. Katsufuji, Transport, magnetic, and structural properties of spinel $MnTi_2O_4$ and the effect of V doping, Phys. Rev. B **74**, 104424 (2006).

[25] A. Rahaman, M. Chakraborty, T. Pramanik, R. K. Maurya, S. Mahana, R. Bindu, D. Topwal, P. Mahadevan, and D. Choudhury, Tetramer orbital ordering and lattice chirality in $MnTi_2O_4$, Phys. Rev. B **100**, 115162 (2019).

[26] S. H. Lee, C. Broholm, T. H. Kim, W. Ratcliff, II, and S. W. Cheong, Local Spin Resonance and Spin-Peierls-like Phase Transition in a Geometrically Frustrated Antiferromagnet, Phys. Rev. Lett. **84**, 3718 (2000).

[27] Ch. Kant, J. Deisenhofer, T. Rudolf, F. Mayr, F. Schrettle, A. Loidl, V. Gnezdilov, D. Wulferding, P. Lemmens, and V. Tsurkan, Optical phonons, spin correlations, and spin-phonon coupling in the frustrated pyrochlore magnets $CdCr_2O_4$ and $ZnCr_2O_4$, Phys. Rev. B **80**, 214417 (2009).

[28] M. C. Kemei, P. T. Barton, S. L. Moffitt, M. W. Gaultois, J. A. Kurzman, R. Seshadri, M. R. Suchomel, and Y.-I. Kim, Crystal structures of spin-Jahn–Teller-ordered $MgCr_2O_4$ and $ZnCr_2O_4$, J. Phys.: Condens. Matter **25**, 326001 (2013).

[29] H. Ueda, H. Mitamura, T. Goto, and Y. Ueda, Successive field-induced transitions in a frustrated antiferromagnet $HgCr_2O_4$, Phys. Rev. B **73**, 094415 (2006).

[30] A. Das, P. Pal, D. Ranaut, K. P. Islam, G. Bhattacharya, S. Mehta, A. Mondal, V. Adyam, K. Mukherjee, A. Das, and D. Choudhury, Origin of the long-range ferrimagnetic ordering in cubic $Mn(Co)Cr_2O_4$, Phys. Rev. B **107**, L100414 (2023).

[31] K. Tomiyasu, J. Fukunaga, and H. Suzuki, Magnetic short-range order and reentrant-spin-glass-like behavior in $CoCr_2O_4$ and $MnCr_2O_4$ by means of neutron scattering and magnetization measurements, Phys. Rev. B **70**, 214434 (2004).

[32] C. Ederer and M. Komelj, Magnetic coupling in $CoCr_2O_4$ and $MnCr_2O_4$: An LSDA + U study, Phys. Rev. B **76**, 064409 (2007).

[33] J. M. Hastings and L. M. Corliss, Magnetic structure of manganese chromite, Phys. Rev. **126**, 556 (1962).

[34] T. Roisnel and J. Rodriguez-Carvajal, WinPLOTR: A Windows tool for powder diffraction pattern analysis, Mater. Sci. Forum, **378-381**, 118 (2000).

[35] K. Dey, S. Majumder, and S. Giri, Ferroelectricity in spiral short-range-ordered magnetic state of spinel $MnCr_2O_4$: Significance of topological frustration and magnetoelastic coupling, Phys. Rev. B **90**, 184424 (2014).

[36] P. C. Hohenberg and B. I. Halperin, Theory of dynamic critical phenomena, Rev. Mod. Phys. **49**, 435 (1977).

[37] J. A. Mydosh, *Spin Glass: An Experimental Introduction* (Taylor & Francis, London, 1993).

[38] R. S. Freitas, L. Ghivelder, F. Damay, F. Dias, and L. F. Cohen, Magnetic relaxation phenomena and cluster glass properties of $La_{0.7-x}Y_xCa_{0.3}MnO_3$ manganites, Phys. Rev. B **64**, 144404 (2001).

[39] A. Kumar, A. Senyshyn, and D. Pandey, Evidence for cluster spin glass phase with precursor short-range antiferromagnetic correlations in the *B*-site disordered $Ca(Fe_{1/2}Nb_{1/2})O_3$ perovskite, Phys. Rev. B **99**, 214425 (2019).

[40] S. Pakhira, N. S. Sangeetha, V. Smetana, A. V. Mudring, and D. C. Johnston, Ferromagnetic cluster-glass phase in $Ca(Co_{1-x}Ir_x)_{2-y}As_2$ crystals, Phys. Rev. B **102**, 024410 (2020).

[41] K. Binder and A. P. J. Young, Spin glasses: Experimental facts, theoretical concepts, and open questions, Rev. Mod. Phys. **58**, 801 (1986).

[42] K. Vlášková, R. H. Colman, P. Proschek, J. Capek, and M. Klicpera, Evidence for spin-glass ground state in fluorite-defect $Er_2Zr_2O_7$ single crystals, Phys. Rev. B **100**, 214405 (2019).

[43] D. Choudhury, P. Mandal, R. Mathieu, A. Hazarika, S. Rajan, A. Sundaresan, U. V. Waghmare, R. Knut, O. Koris, P. Nordblad, and D. D. Sarma, Near-Room-Temperature Colossal Magnetodielectricity and Multiglass Properties in Partially Disordered La_2NiMnO_6, Phys. Rev. Lett. **108**, 127201 (2012).

[44] M. Giot, A. Pautrat, G. Andre, D. Saurel, M. Hervieu and J. Rodriguez-Carvajal, Magnetic states and spin-glass properties in $Bi_{0.67}Ca_{0.33}MnO_3$: Macroscopic ac measurements and neutron scattering, Phys. Rev. B **77**, 134445 (2008).

[45] R. C. Sahoo, Y. Takeuchi, A. Ohotomo, and Z. Hossain, Exchange bias and spin glass states driven by antisite disorder in the double perovskite compound $LaSrCoFeO_6$, Phys. Rev. B **100**, 214436 (2019).

[46] S. Pal, K. Kumar, A. Banerjee, S. B. Roy and A. K. Nigam, Field-cooled state of the canonical spin glass revisited, Phys. Rev. B **101**, 180402(R) (2020).

[47] C. Leighton, J. Nogues, B. J. Jonsson-Akerman, and I. K. Schuller, Coercivity Enhancement in Exchange Biased Systems Driven by Interfacial Magnetic Frustration, Phys. Rev. Lett. **84**, 3466 (2000).

[48] E. Choi, G.-W. Chern, and N. B. Perkins, Chiral magnetism and helimagnons in a pyrochlore antiferromagnet, Phys. Rev. B **87**, 054418 (2013).

[49] A. P. Ramirez, Geometrical frustration in magnetism, Czech. J. Phys. **46**, 3247 (1996).

[50] John E. Greedan, Geometrical frustration in magnetism, J. Mater. Chem. **11**, 37 (2001).

[51] P. Schiffer and A. P. Ramirez, Recent experimental progress in the study of geometrical magnetic frustration, Comments. Cond. Mat. Phys. **18**, 21 (1996).

[52] T. Katsufuji, S. Mori, M. Masaki, Y. Moritomo N. Yamamoto, and H. Takagi, Dielectric and magnetic anomalies and spin frustration in hexagonal $RMnO_3$ (R = Y, Yb, and Lu), Phys. Rev. B **64**, 104419 (2001).

[53] M. Das, S. Roy, N. Khan, and P. Mandal, Giant magnetocaloric effect in an exchange-frustrated $GdCrTiO_5$ antiferromagnet, Phys. Rev. B **98**, 104420 (2018).

[54] V. Kocsis, Y. Tokunaga, T. Room, U. Nagel J. Fujioka, Y. Taguchi, Y. Tokura, and S. Bordacs, Spin-Lattice and Magnetoelectric Couplings Enhanced by Orbital Degrees of Freedom in Polar Multiferroic Semiconductors, Phys. Rev. Lett. **130**, 036801 (2023).

[55] C. dela Cruz, F. Yen, B. Lorenz, Y. Q. Wang Y. Y. Sun, M. M. Gospodinov, and C. W. Chu, Strong spin-lattice coupling in multiferroic $HoMnO_3$: Thermal expansion anomalies and pressure effect, Phys. Rev. B **71**, 060407(R) (2005).

[56] K. Dey, A. Karmakar, S. Majumder, and S. Giri, Strong magnetoelastic coupling and unconventional electric polarization in the triangular-lattice multiferroic $Li_{0.99}Cu_{0.01}CrO_2$, Phys. Rev. B **87**, 094403 (2013).

[57] A. Pal, C. H. Huang, T. W. Yen, P. H. Lee, Y. H. Chang, C. H. Yeh, T. W. Kuo, A. Tiwari, D. C. Kakarla, S. M. Huang, M. C. Chou, H. S. Kunwar, S. Rana, V. G. Sathe, B. H. Chen, Y. C. Chuang, and H. D. Yang, Spin-induced strongly correlated magnetodielectricity, magnetostriction effect, and spin-phonon coupling in helical magnet $Fe_3(PO_4)_3O_3$, Phys. Rev. B **106**, 094404 (2022).

[58] M. C. Kemei, S. L. Moffitt, L. E. Darago, R. Seshadri M. R. Suchomel, D. P. Shoemaker, K. Page, and J. Siewenie, Structural ground states of $(A, A\prime)Cr_2O_4$ (A = Mg, Zn; $A\prime$ = Co, Cu) spinel solid solutions: Spin-Jahn-Teller and Jahn-Teller effects, Phys. Rev. B **89**, 174410 (2014).

[59] M. R. Suchomel, D. P. Shoemaker, L. Ribaud, M. C. Kemei, and R. Seshadri, Spin-induced symmetry breaking in orbitally ordered $NiCr_2O_4$ and $CuCr_2O_4$, Phys. Rev. B **86**, 054406 (2012).